ISBN: 978-3-95450-236-3 ISSN: 2673-5350 doi:10.18429/JACoW-IBIC2023-TUP011

GEOMETRY STUDY OF AN RF-WINDOW FOR A GHz TRANSITION RADIATION MONITOR FOR LONGITUDINAL BUNCH SHAPE MEASUREMENTS

S. Klaproth*[1], A. Penirschke, Technische Hochschule Mittelhessen, Friedberg, Germany
R. Singh, GSI Helmholtzzentrum für Schwerionenforschung, Darmstadt, Germany
H. De Gersem, Technische Universität Darmstadt, Darmstadt, Germany
[1]also at Technische Universität Darmstadt, Darmstadt, Germany

Abstract

GHz Transition Radiation Monitors (GTRs) can be used to measure longitudinal beam profiles even for low β beams. In contrast to traditional methods e.g., Fast Faraday Cups (FFCs) and Feschenko monitors, GTRs are a non-destructive measurement method and are able to resolve bunch-by-bunch longitudinal profiles at the same time. It is planned to measure the transition radiation outside the beam line through a custom-design RF window within a frequency range up to 8 GHz using broadband antenna structures. The material and the shape of the RF-window is crucial in order to minimize the fraction of the transition radiation that is not propagating in the direction of the antenna. In this contribution, we show a study of different geometries to suppress reflections generated at the transition to the RF-window. For higher permittivity the reflections becomes stronger, simultaneously reducing the measured signal strength at the position of the antenna. Secondly the RF-window's material must be UHV compatible and should be durable.

INTRODUCTION

The longitudinal bunch shape is important for conditioning and verifying the beam dynamics of LINACs. In the case of the GSI UNILAC, the bunch velocities β typically range from 0.05 to 0.15. For these slow bunches, the self-field widens significantly alongside the beam axis, rendering direct measurement of the longitudinal bunch shape inherently ambiguous [1]. This applies to devices such as phase probes and other pick-ups. Therefore, more common tools for longitudinal bunch shape measurements of low-beta beams are FFCs and Feschenko monitors.

FFCs measure the profile by collecting the bunch charge in a 50 Ω optimized cup. Typically, the beam's self-fields are shielded to suppress signal widening caused by early arriving fields on the collector. This enables FFCs to detect the bunch shape with high precision on a bunch-by-bunch basis. Additional considerations must be taken on the emission of secondaries during the design phase and later on while interpreting the measured signals. Nevertheless, the destructive measurement makes a further usage of the beam impossible [2–4].

Feschenko monitors, on the other hand, measure the average bunch shape. The beam passes by a thin wire generating secondary electrons. The longitudinal structure of the beam is coherently transformed to the transversal distribution of these secondaries using an RF-deflector [2, 5]. The interaction of the beam and the wire is minimal, allowing the bunches to remain suitable for further acceleration.

A new candidate for bunch shape measurements is the GTR. This type of device is still under investigation, but has the potential to combine the advantages of both FFCs and Feschenko monitors, enabling bunch-by-bunch measurements without beam destruction. The GTR comprises three major components: a metal target plate with an aperture to generate transition radiation while the beam passes through, an RF-window for decoupling the transition radiation from the inner beam line to the outside simultaneously maintaining the vacuum, and an antenna/coupler structure to observe the radiation as seen in Fig. 1. This promising concept has

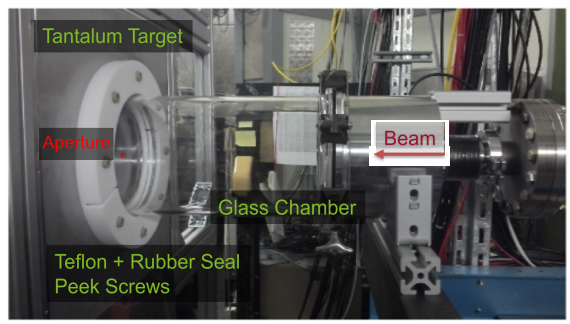

Figure 1: Experimental Setup of the proof-of-concept measurements [6].

been tested successfully at GSI [6]. Consequently, further investigations were made to optimize the RF window in the current setup. Simulations were carried out using different possible materials for the RF window, both ideal [7] and realistic [8], to examine their influence on the expected transition radiation signal. Thereby, a cylindrical RF-window with a wall thickness of 10 mm analog to the proof-of-concept measurement has been used. In Fig. 2a,b, we illustrate the expected maximum peak field (E_{max}) for two different typical β values at GSI UNILAC. It becomes evident, that a low relative permittivity ϵ_r is advantageous for maximizing the expected signal amplitude. The antenna should be positioned at an angle θ at least above 40°. As a rule of thumb for high β beams, $\theta = \frac{1}{\gamma}$ provides a good approximation for the angle at which the transition radiation peak power is emitted [10]. In case of GSI UNILAC this corresponds to approximately 55° to 60°. But actually at these low β values the maximum intensity rises continuously towards

* Stephan.Klaproth@iem.thm.de

ISBN: 978-3-95450-236-3 ISSN: 2673-5350 doi:10.18429/JACoW-IBIC2023-TUP011

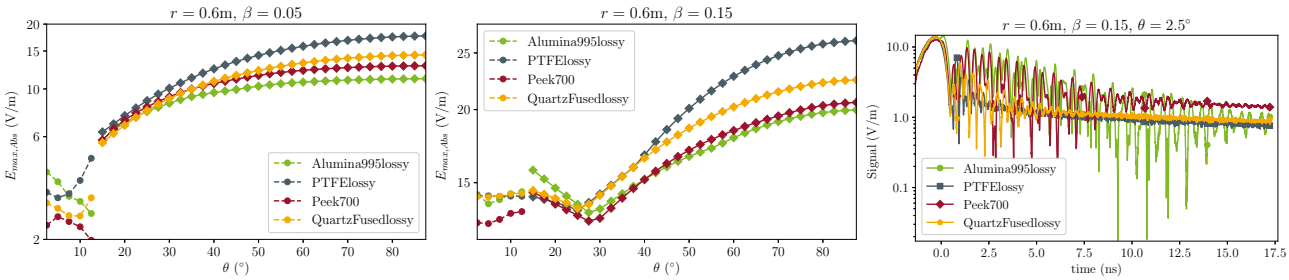

(a) (b) (c)

Figure 2: The maximum amplitude of the transition radiation peak $E_{\max}$ at 0.6 m distance for (a) $\beta = 0.05$ and (b) $\beta = 0.15$ and (c) the reflections after the transition radiation passed for different realistic materials [9]. A circle marker identifies an observation position inside and a diamond outside the vacuum chamber.

the target as shown in Fig. 2a and 2b. It can be noticed that only the necessary geometric distance of the antenna to the target gives an upper bound to the positioning angle θ.

$$\vec{E} = \frac{q \cdot \beta}{2\pi\epsilon_0 c_0 |\vec{R}|} \frac{\sin\theta\,\delta\left(|\vec{R}|c_0^{-1} - t\right)}{1 - \beta^2\cos^2\theta} (\hat{e}_x \cos\theta + \hat{e}_z \sin\theta)\,. \quad (1)$$

The electrical field of transition radiation for a single charge in the far-field may be calculated using Eq. (1) [11]. It shows that signal strength increases linearly with higher β values. Therefore, the optimal position for the antenna should be chosen with respect to the lowest expected β case to achieve the best overall performance of the GTR. The performance also depends on the suppression of reflections. Consequently, the spacing between the bunches defines a time gap within which reflections shall relax to prevent interference with the measured signal of the following bunch. The UNILAC operates at 36 MHz to 108 MHz, corresponding to a spacing of 27.78 ns to 9.26 ns between two consecutive bunches. In Fig. 2c we illustrate the signal within the vacuum chamber at $|\vec{R}| = 0.6$ m and $\theta = 2.5°$ at a velocity $\beta = 0.15$. The simulation time has been adjusted so that zero aligns with the transition radiation peak to be measured, followed by its reflections. While the reflections fade away for all materials within 27.78 ns for all materials, the faster operation mode of 108 MHz may encounter interference between the transition radiation of the following bunch and the reflections of the current one, depending on the RF-window material used. A well-chosen material can minimize this interaction. For instance, the reflection amplitude and relaxation time of quartz-glass perform similarly well compared to PTFE, while Peek and Alumina suffer significantly from slowly decaying reflections within the vacuum chamber. For the quartz-glass RF-window the expected total relaxation time is about 7.5 ns, which is shorter than the time gap of the fast operation mode of the UNILAC. So we do not expect severe impacts on the following measured bunch shape due to reflections of the previous transition radiation. The impact of the transition radiation on the following bunch itself is also expected to be negligible, with electric fields of about 100 V m^{-1} compared to the self-fields of the bunch, typically in the range of tens to hundreds of kV m^{-1}. Both low ϵ_r materials would be sufficient in terms of their electrical properties. But the material class PTFE is typically used only inside a vacuum chamber or for low vacuum applications, as it may not be vacuum-tight against hydrogen and other light particles [12, 13]. Therefore, we focus in our geometry study on the quartz-glass material only. During this geometry study of the RF-window our aim is to increase the amplitude of the measured signal outside the vacuum chamber while reducing the amplitude and relaxation time of the reflections inside the beam line to further minimize their impact on the measurements.

SIMULATIONS

Several shapes were evaluated using the CST® PIC-solver [9]. The first shape is a cylindrical design, which was also used in the material analysis, and it includes a larger variant with a 0.5 m inner radius (Fig. 3a). The second shape is a spherical geometry with an inner radius of 0.5 m (Fig. 3b). The highest transmission through the window is expected when the transition radiation impinges orthogonally on the window surface.

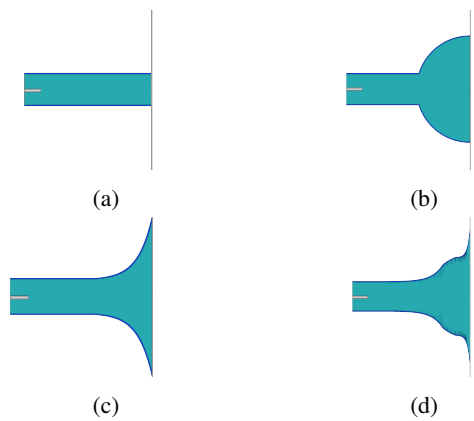

(a) (b) (c) (d)

Figure 3: The shapes studied: (a) cylindrical, (b) spherical, (c) exponential horn, (d) combination of spherical and exponential horn design.

The third shape is an exponential horn (Fig. 3c) with a mouth of 0.5 m. This shape is intended to disperse the transition radiation as much as possible to create only low amplitude reflections. The last shape is a combination of

ISBN: 978-3-95450-236-3 ISSN: 2673-5350 doi:10.18429/JACoW-IBIC2023-TUP011

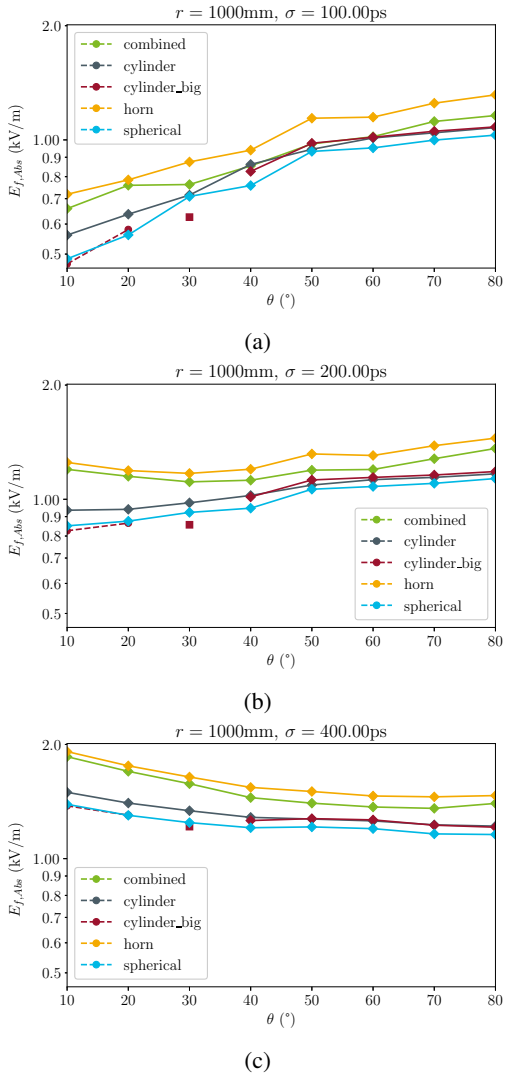

Figure 4: Maximum signal strength of the transition radiation $E_{\max}$ at 1 m distance for different geometries and bunch lengths: (a) $\sigma_b = 100$ ps, (b) $\sigma_b = 200$ ps, (c) $\sigma_b = 400$ ps. A circle marker identifies an observation position inside and a diamond outside of the vacuum chamber and a square identifies an observer within the chamber walls.

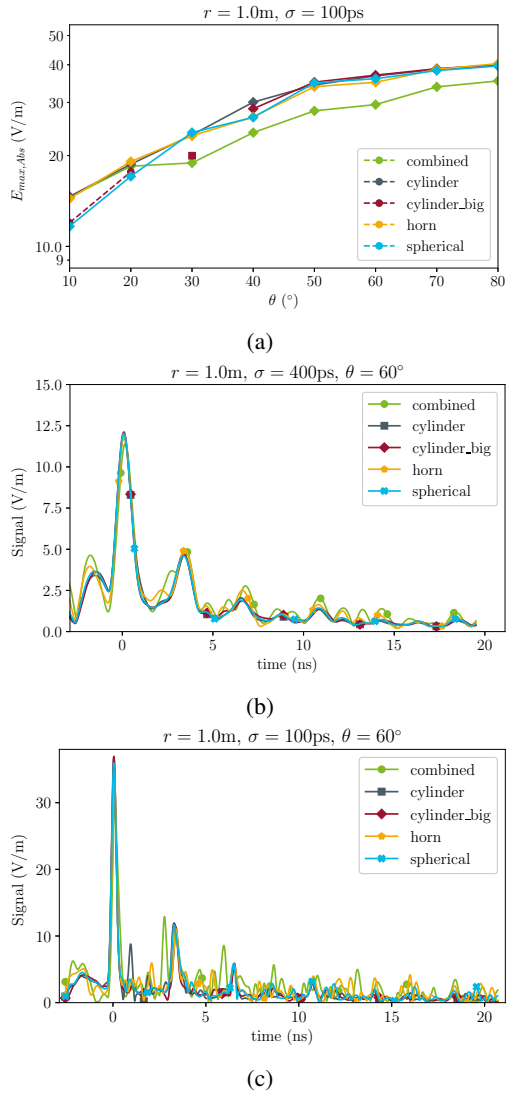

Figure 5: Signal of the transition radiation inside the RF-window in (a) at $|\vec{R}| = 0.4$ m and $\theta = 0°$ for a $\sigma_b = 400$ ps bunch and outside at $|\vec{R}| = 1$ m and $\theta = 60°$ for (b) $\sigma_b = 400$ ps and (c) $\sigma_b = 100$ ps bunch.

exponential horn and spherical shape (Fig. 3d). The spherical part spans between 50° to 70° with an inner radius of 0.4 m and is enclosed by two exponential horn sections. In all cases the wall thickness is kept to 10 mm using fused-quartz-glass as RF-window material simulating 10^{10} single charged particles in a Gaussian shaped bunch.

In Fig. 4 the maximum intensity of the transition radiation is plotted against the observation angle θ at a distance of $|\vec{R}| = 1$ m for $\beta = 0.15$ across all geometries, considering three different bunch lengths. Clearly the combined shape performs subpar compared to all other geometries. The maximum intensity increases with θ for both shorter bunches (Fig. 4a, 4b), as well as for the $\sigma_b = 400$ ps case till $\theta = 60°$. Beyond this angle the maximum intensity of the transition radiation stagnates for longer bunches. The exponential horn geometry shows a slightly lower maximum amplitude compared to the cylindrical and spherical shapes, but the difference is negligible. Notably, the maximum intensity scales linearly with the bunch charge density [11], as expected. All simulations have been performed with the same total charge, resulting in a halving of the bunch charge density between bunch lengths of $\sigma_b = 100$ ps to 200 ps. Consequently, the maximum intensity also decreases by half, from approximately 40 V m^{-1} to 20 V m^{-1}, and quartered from about 40 V m^{-1} to 10 V m^{-1} for $\sigma_b = 100$ ps to 400 ps. In Fig. 5a we show the signal of the transition radiation and reflections along the beam axis at a distance of $|\vec{R}| = 0.4$ m from the target for a σ_b=400 ps bunch. For the first 6 ns, the spherical geometry has a higher amplitude than the horn-shaped RF-window. Afterward, the reflections become even smaller in amplitude. In the case of the small cylindrical shape, the signal appears to have a low reflectivity. However, this is due to the overlap between the first reflection

ISBN: 978-3-95450-236-3 ISSN: 2673-5350 doi:10.18429/JACoW-IBIC2023-TUP011

and the actual transition radiation signal. As a result, the transition radiation signal broadens, and the maximum amplitude shifts. This first reflection becomes visible in the big cylindrical shape case around 4 ns. Here, the longer travel distance of the reflection leads to the delayed signal and therefore the reflection is separated from the transition radiation. The widening of the transition radiation signal also occurs for the horn-shaped geometry, with a small kink visible after 1.9 ns. This kink is caused by reflections at the outer part of the horn mouth, where the gap between the target and RF-window is small. These early reflections overlap with the transition radiation, ultimately leading to a widening. The primary peak of the reflected transition radiation inside the RF-window can be reduced by up to 12 % comparing the highest amplitude of the spherical and the lowest of horn shape. The transition radiation peak of the following bunch will interact with the remaining reflections at 9.26 ns, which represents a minimum. So, we do not expect significant interference effects between the reflected signals of consecutive bunches. To further confirm this, additional multi-bunch simulations are required. In Fig. 5b,c the signal outside the RF-window is shown at $\theta = 60°$ in $|\vec{R}| = 1$ m distance at $\beta = 0.15$ for two bunch widths of $\sigma_b = 400$ ps and 100 ps. The aim outside the RF-window is to maximize the transition radiation signal. With the exception of the combined shape, all geometries exhibit nearly the same amplitude. This is particularly pronounced in the $\sigma_b = 100$ ps case, where the amplitude is approximately 25 % smaller than the others. In Fig. 5c, the first reflection of the small cylindrical geometry becomes visible approximately 1 ns after the main peak. This reflection overlaps in the $\sigma_b = 400$ ps case leading to the widening of the signal as discussed already earlier. Additionally, the early reflection of the horn shape can be seen between 1 ns to 3 ns, resulting in the kink for longer bunches. The best separation between the signal and reflections is achieved with the spherical and the larger cylindrical geometries. In terms of relaxation time τ we perform an exponential fit

$$s(t) = s_0 \exp^{\frac{-t}{\tau}} + C, \quad (2)$$

with s_0 the maximum amplitude of the primary transition radiation peak and the increased noise floor offset C. The results of the fit are shown in in Fig. 6. The horn-geometry's decay time τ is the smallest on average with 2.7 ns, but the increased noise floor C is one of the worst together with the combined shape up to 2 V m^{-1} higher than the other geometries. All other shapes have a decay time τ of about 3 ± 0.3 ns with a small advantage for the spherical and the larger cylindrical shape. The smallest increased noise floor C of about 1.1 ± 0.1 V m^{-1} is achieved with the big cylindrical shape, followed closely by the spherical geometry 1.4 ± 0.3 V m^{-1}.

CONCLUSION

In this paper, we have demonstrated that the permittivity of the RF-window has a significant impact on the reflections of the transition radiation in a GTR. Additionally, we showed that the shape of the window does not have a major effect on the measurable intensity of the transition radiation outside the RF-window. Inside the RF-window, the horn geometry can reduce the amplitude by up to 12 % at the cost of a slightly widened signal. The lowest decay time τ and increased noise floor C are achieved with the bigger cylindrical and the spherical designs. The advantage of the alternative geometries are the ability to separate the transition radiation from the reflections, with the horn geometry offering some improvement and the spherical shape performing best in this regard. We plan to equip a GTR with a spherical shaped RF-window to test its influence in a new measurement campaign also adding antennas with higher bandwidth up to 8 GHz bandwidth. Furthermore, simulations of multiple bunches will be performed to compare with measurements with respect to the overlapping of reflections and the desired transition radiation peaks.

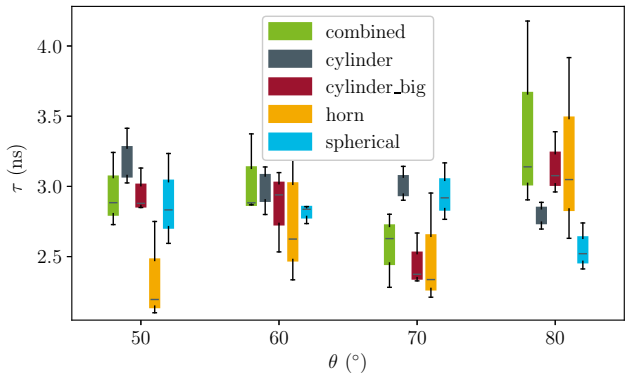

(a)

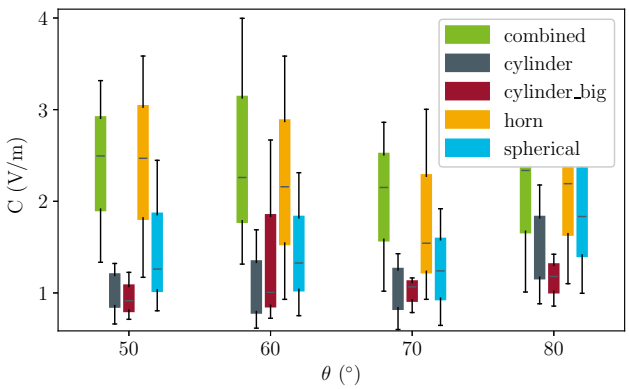

(b)

Figure 6: (a) Decay constant τ and (b) offset C of the exponential decay fit averaged over σ_b (100, 200, 400 ps) for each angle θ.

ACKNOWLEDGEMENTS

This work is supported by the German Federal Ministry of Education and Research (BMBF) under contract no. 05P21RORB2. Joint Project 05P2021 - R&D Accelerator (DIAGNOSE).

ISBN: 978-3-95450-236-3 ISSN: 2673-5350 doi:10.18429/JACoW-IBIC2023-TUP011

REFERENCES

[1] P. Forck, P. Kowina, and D. Liakin, "Beam Position Monitors," *Synchrotron Radiation News*, vol. 1, no. 3, 2008. https://www.researchgate.net/publication/236630408_Beam_Position_Monitors

[2] R. Singh *et al.*, "Comparison of Feschenko BSM and Fast Faraday Cup with Low Energy Ion Beams," in *Proc. IBIC'21*, Pohang, Rep. of Korea, Oct. 2021, pp. 407–411. doi:10.18429/JACoW-IBIC2021-WEPP16

[3] R. Singh, P. Forck, S. Klaproth, T. Reichert, A. Reiter, and G. O. Rodrigues, "Simulation and Measurements of the Fast Faraday Cups at GSI UNILAC," in *Proc. IBIC'22*, Kraków, Poland, Dec. 2022, pp. 286–290. doi:10.18429/JACoW-IBIC2022-TUP25

[4] K. Mal, S. Kumar, G. Rodrigues, and R. Singh, "Study and improvements of a radially coupled coaxial Fast Faraday cup design toward lower intensity beams," *AIP Advances*, vol. 12, no. 12, p. 125 223, Dec. 2022. doi:10.1063/5.0131890

[5] A. Feschenko, "Methods and instrumentation for bunch shape measurements," in *Proc. PAC'01*, Chicago, IL, USA, vol. 1, 2001, pp. 517–521. https://jacow.org/p01/PAPERS/ROAB002.PDF

[6] R. Singh, T. Reichert, and B. Walasek-Hoehne, "Optical transition radiation based transverse beam diagnostics for nonrelativistic ion beams," *Phys. Rev. Accel. Beams*, vol. 25, no. 7, p. 072 801, Jul. 2022. doi:10.1103/PhysRevAccelBeams.25.072801

[7] S. Klaproth, H. D. Gersem, A. Penirschke, T. Reichert, and R. Singh, "Advancing to a GHz Transition Radiation Monitor for Longitudinal Charge Distribution Measurements," in *Proc. IPAC'22*, Bangkok, Thailand, Jul. 2022, pp. 267–270. doi:10.18429/JACoW-IPAC2022-MOPOPT018

[8] S. Klaproth, H. D. Gersem, and A. Penirschke, "Analysis of Real Materials for the RF Window of a GHz Transition Radiation Monitor," DPG-Frühjahrstagung SMUK23 - AKBP 17.5, Mar. 2023.

[9] *CST Studio Suit 2023™ SP5*. https://www.3ds.com/products-services/simulia/products/cst-studio-suite/

[10] L. C. L. Yuan, C. L. Wang, H. Uto, and S. Prünster, "Formation-Zone Effect in Transition Radiation Due to Ultrarelativistic Particles," *Phys. Rev. Lett.*, vol. 25, no. 21, pp. 1513–1515, Nov. 1970. doi:10.1103/PhysRevLett.25.1513

[11] R. Singh, "Longitudinal Beam Diagnostics R&D at GSI-UNILAC," in *Proc. HIAT'22*, Darmstadt, Germany, Aug. 2022, paper TH2I2, pp. 144–149. doi:10.18429/JACoW-HIAT2022-TH2I2

[12] B. Sebők, M. Schülke, F. Réti, and G. Kiss, "Diffusivity, permeability and solubility of H2, Ar, N2, and CO2 in poly(tetrafluoroethylene) between room temperature and 180°C," *Polymer Testing*, vol. 49, pp. 66–72, 2016. doi:10.1016/j.polymertesting.2015.10.016

[13] G. Lee, *Materials for ultra-high vacuum*, UNT Digital Library - online, Aug. 1989. https://digital.library.unt.edu/ark:/67531/metadc1185924/